

## Heavy-Ion-induced Defects in Degraded SiC Power MOSFETs

Corinna Martinella<sup>1,a\*</sup>, Marianne Bathen<sup>1,b</sup>, Arto Javanainen<sup>2,3,c</sup>,  
 Ulrike Grossner<sup>1,d</sup>

<sup>1</sup>Advanced Power Semiconductor Laboratory, ETH Zurich, 8092 Zurich, Switzerland

<sup>2</sup>Department of Physics, University of Jyväskylä, FI-40014 Jyväskylä, Finland

<sup>3</sup>Electrical Engineering and Computer Science Dep., Vanderbilt University, Nashville, TN 37235  
 USA

<sup>a</sup>martinella@aps.ee.ethz.ch, <sup>b</sup>bathen@aps.ee.ethz.ch, <sup>c</sup>arto.javanainen@jyu.fi,

<sup>d</sup>ulrike.grossner@ethz.ch

**Keywords:** Single Event Effects, Heavy-Ions, SiC Power MOSFETs, Defects

**Abstract.** Cathodoluminescence spectroscopy is used to investigate the formation of point- and extended defects in SiC power MOSFETs exposed to heavy-ions. Devices showing single event leakage current (SELC) effects are analysed and compared to pristine samples. Common luminescence peaks of defect centers localized in the thermal-SiO<sub>2</sub> are identified, together with peaks at the characteristic wavelength of extended defects.

### Introduction

The reliability of a SiC power MOSFET exposed to cosmic rays, as in space applications, depends on the operational drain-source bias ( $V_{DS}$ ) and on the linear energy transfer (LET) of the particle. During the recent years, many studies have been performed to investigate the effects of heavy-ions in SiC power devices, highlighting the susceptibility of this technology to different single event effects (SEEs) [1-8]. A summary of the SEEs observed for SiC power MOSFETs from the 2<sup>nd</sup> Gen. Cree/Wolfspeed exposed to heavy ions (for  $LET > 7 \text{ MeVcm}^2/\text{mg}$ ) is shown in Fig. 1, after [4].

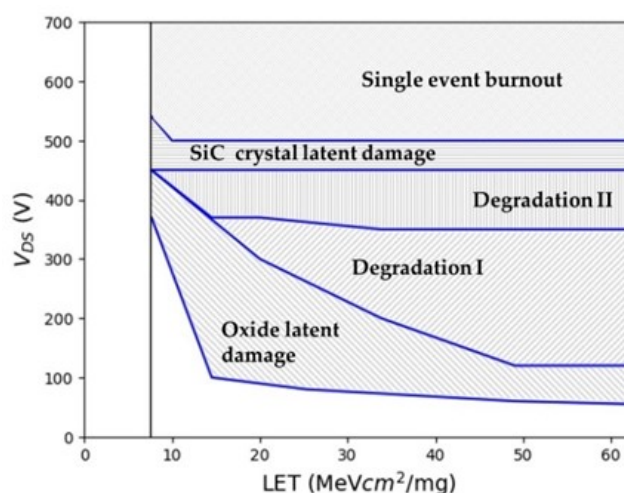


Fig. 1: Summary of radiation responses of SiC power MOSFETs with planar gate from the 2<sup>nd</sup> Gen. Cree/Wolfspeed, as a function of the drain-source bias during the exposure and the ion LET, after [4].

When a low  $V_{DS}$  is applied during the irradiation (at  $V_{GS}=0$  V) only a temporal increase in leakage current is observed during the exposure due to collection of additional charges created by the incoming particles. However, over a certain threshold, latent damage is created in the gate oxide which can induce a failure of the component when performing a post-irradiation-gate-stress (PIGS) test. The

$V_{DS}$  and LET conditions at which this effect is observed define the area named “oxide latent damage” in Fig. 1. Increasing the  $V_{DS}$  over a second threshold, a permanent increase of gate and drain leakage currents is measured directly during the irradiation. This effect is non-destructive, and it is commonly referred to as degradation or, as recently named, single event leakage current (SELC). From microbeam experiments [8], two sub-regions have been identified for SELC. Initially, the drain and gate leakage currents increase with the same magnitude, and the area beneath the gate (JFET and channel regions) is the most sensitive (“degradation I”). At higher  $V_{DS}$ , additional drain leakage current is observed in the p-n junction region (“degradation II”). This second mechanism of degradation was suggested to be the same as observed in SiC Schottky diodes and to be caused by Joule heating, which results in increasing temperature and phase change in the SiC substrate, as confirmed by molecular dynamics (MD) simulations [9-10]. These regions are unlikely to recover completely, leaving permanent structural modification in the SiC lattice, causing the creation of permanent extended defects (ED) (e.g., different SiC polytype inclusions, stacking faults, dislocations, clusters, etc.). This effect can also lead to a destructive failure when sweeping the  $V_{DS}$  after the irradiation (“SiC crystal latent damage”). Finally, at higher  $V_{DS}$  a destructive single event burnout (SEB) is observed during the exposure (at  $V_{DS} \sim 500$  V for these devices [3]).

There is still a lack of understanding concerning the creation of defects when observing SEEs in SiC power MOSFETs. The objective of this work is to use cathodoluminescence (CL) spectroscopy to investigate and identify the heavy-ion-induced defects created when observing the first and second type of degradation.

## Experimental Method

**Heavy-ion irradiation.** The experiment was carried out at the RADiation Effects Facility (RADEF) in the Accelerator Laboratory of the University of Jyväskylä, Finland.  $^{56}\text{Fe}^{+15}$  and  $^{131}\text{Xe}^{+35}$  ions were selected from the 16.3 MeV/amu cocktail, having a beam size of  $2 \times 2$  cm<sup>2</sup>. The ion characteristics and the irradiation conditions are reported in Table 1. Bare die from the 2<sup>nd</sup> generation Cree/Wolfspeed rated for 1.2 kV and with  $R_{DS(ON)} = 80$  m $\Omega$  were selected as devices under test (DUTs) (CPM2-1200-0080B). The same setup as described in [4] was used for this experiment. Each bare die was exposed at normal incidence of the beam with respect to the device surface. The devices were irradiated at constant  $V_{DS}$  and  $V_{GS} = 0$  V during each run. After each irradiation the  $V_{DS}$  was increased, until a maximum voltage reported in the 6<sup>th</sup> column of Table 1. Two devices were considered for CL analysis; DUT 1 degraded with SELC I (degradation I) and DUT 2 degraded with SELC II (degradation II).

Table 1: Conditions of irradiation.

DUT	Ion	Energy [MeV]	LET@Surface [MeVcm <sup>2</sup> /mg]	Range SiC [ $\mu$ m]	Max $V_{DS}$ [V]	Fluence [ion/cm <sup>2</sup> ]	SEE
1	$^{57}\text{Fe}^{20+}$	941	14.64	136.4	270	$3 \times 10^6$	SELC I
2	$^{126}\text{Xe}^{44+}$	2059	49.10	112.2	400	$7 \times 10^6$	SELC II

**Cathodoluminescence spectroscopy.** After the irradiation the devices were prepared for the cathodoluminescence (CL) analysis. A bond tester was used to remove the wires from the gate and source pads. Successively, a hot plate set at 110 °C was used to melt the solder paste and unsolder the devices from the board. Then, the Al layers covering the source and drain regions were removed by placing the two samples in a 1:5 diluted KOH etch for 40 min. CL spectroscopy was used to investigate the nature of defects created during the irradiations. CL makes use of focused electron beams to probe the electronic transitions resulting in the emission of characteristic light in a wide spectral range [11]. The measurements were carried out using a JEOL JSM-IT300 scanning electron microscope (SEM) equipped with a LaB<sub>6</sub> filament and a Delmic SPARC CL system integrated in the SEM chamber. Hyperspectral data

was collected with an Andor Shamrock SR-193i spectrometer with a 300 l/mm grating and a CCD Andor Newton DU940P-BU2 detector. The CL spectra were collected at 80 K using a probe current of 0.08 nA to 0.12 nA and a 20 kV acceleration voltage, allowing collection of signals from up to  $1\text{ }\mu\text{m}$  depth. The signal was collected using different dimensions for each pixel, ranging from  $1 \times 1\text{ }\mu\text{m}^2$  to  $20 \times 20\text{ }\mu\text{m}^2$  (for reference, the cell pitch of the unit cell is  $9.1\text{ }\mu\text{m}$ ). In addition to the irradiated devices, a pristine sample from the same manufacturer and generation (a  $25\text{ m}\Omega$  device) was used as a reference for comparison. The pristine reference showed in the next section was calculated as the average of three pixels (high, medium and low intensity), selecting different pixel sizes depending on the comparison.

## Results and Discussion

The first CL analysis was performed on the etched-back bare die surface for the irradiated samples, an example is shown in Fig. 2. The first DUT was exposed to  $^{56}\text{Fe}^{+15}$  and degraded with SELC I whereas the second DUT analysed was exposed to  $^{131}\text{Xe}^{+35}$  and degraded with SELC II. The pixel sizes used to collect the light emission with a depth of  $1\text{ }\mu\text{m}$  were respectively  $1 \times 1\text{ }\mu\text{m}^2$  and  $20 \times 20\text{ }\mu\text{m}^2$  for the two devices. The CL false color maps reported in Figs. 2 (a) and 2 (b) display the relative intensity across the probed area for a 29.7 nm broad spectral region centered at 471 nm and 466 nm, respectively. Brighter regions, highlighted in Pixels 1 and 3 for both DUTs, are observable within a distance of  $\sim 200\text{ }\mu\text{m}$  for DUT 1 and  $\sim 32\text{ }\mu\text{m}$  for DUT 2 and represent areas with higher intensity emission in the  $\sim 470 \pm 15\text{ nm}$  spectra region. For both samples, Pixel 2 was selected to represent an intermediate signal, whereas Pixel 4 is taken sufficiently distant from the brighter area as reference for the background level. It is hypothesized that the higher intensities observed in Pixels 1 and 3 for DUT 1 and DUT 2 are induced by ion tracks and therefore the surrounding areas provide information concerning the extension of the damage, which appears to be substantially larger for the DUT 2 which was exposed to  $^{131}\text{Xe}^{+35}$  and degraded with SELC II. The different distances between the possible ion tracks for the  $^{56}\text{Fe}^{+15}$  and  $^{131}\text{Xe}^{+35}$  exposures could be explained by random irradiation events. In Figs. 2(c) (DUT 1: SELC I,  $^{56}\text{Fe}^{+15}$ ) and 2(d) (DUT 2: SELC II,  $^{131}\text{Xe}^{+35}$ ) the corresponding CL signals collected for Pixels 1-4 are presented as a function of the wavelength. A pristine reference calculated as the average of three pixels of the same size is also reported for comparison. All spectra exhibit the near band edge emission of 4H-SiC (onset at  $\sim 390\text{ nm}$ ) along with defect related features. For both samples, common luminescence peaks of defect centers localized in the thermal-SiO<sub>2</sub> are identifiable as reported in literature, such as oxygen vacancy centers (OVCs) at  $\sim 445\text{-}480\text{ nm}$  [12] and non-bridging oxygen hole centers (NBOHCs) at  $\sim 660\text{ nm}$  [12-13]. Si-N bonding structures at  $\sim 580\text{ nm}$  [13] are observed in DUT 2 (see Fig. 2 (d)). Point defect related features were not observed in the near infrared region extending to  $900\text{ nm}$  wavelength, including the AB-lines attributed to the carbon antisite-vacancy pair [13] and the V-lines assigned to the Si vacancy [14]. From the molecular dynamics simulations, the maximum temperature at  $20\text{ nm}$  from the track is reported to reach  $2000\text{ K}$  (bias of  $150\text{ V}$  [10]). At such temperatures, the immediate out-annealing of point defects such as vacancies and interstitials is expected, leaving only more extended lattice damage behind. In addition, a series of interesting features are observed in different regions of DUT 1 (SELC I,  $^{56}\text{Fe}^{+15}$ ). Fig. 3 (a) displays the false color map for a  $31\text{ nm}$  broad spectral region centered at  $575\text{ nm}$ , with a pixel size of  $3 \times 3\text{ }\mu\text{m}^2$ . The four brightest pixels are selected on the map. All of them are in-between the gate stripes. In addition to the OVC and NBOHC peaks already discussed, higher emission of defects that are possibly related to Si-N structures at  $\sim 580\text{ nm}$  [12] are marked by a vertical line in Fig. 3 (b) for the four spectra. In this case, the intensity of the peaks identified as Si-N bonding structures are comparable with the intensity of the OVC and NBOHC peaks. Such comparable emissions was not observed in the pristine sample or the DUT 2 (SELC II,  $^{131}\text{Xe}^{+35}$ ), even when using the same pixel size of  $3 \times 3\text{ }\mu\text{m}^2$ .

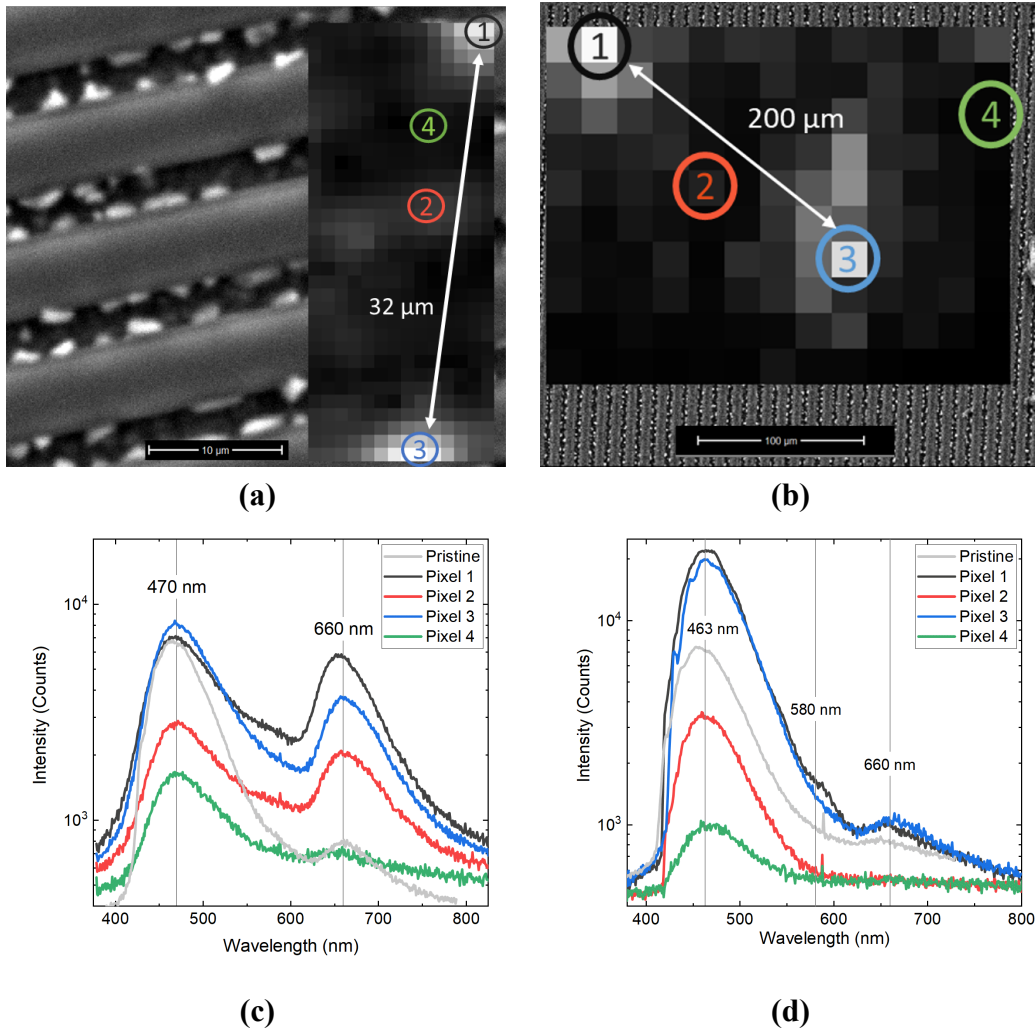


Fig. 2: Panels (a) and (b) show CL false color maps for DUT 1 and DUT 2 respectively with pixel sizes of  $1 \times 1 \mu\text{m}^2$  and  $20 \times 20 \mu\text{m}^2$  showing the relative intensity for a 29.7 nm broad spectral region centered at 471 nm and 466 nm, respectively. In (c) and (d) the CL spectrum as a function of the wavelength is shown for the four pixels selected in (a) and (b) and a pristine reference (in gray).

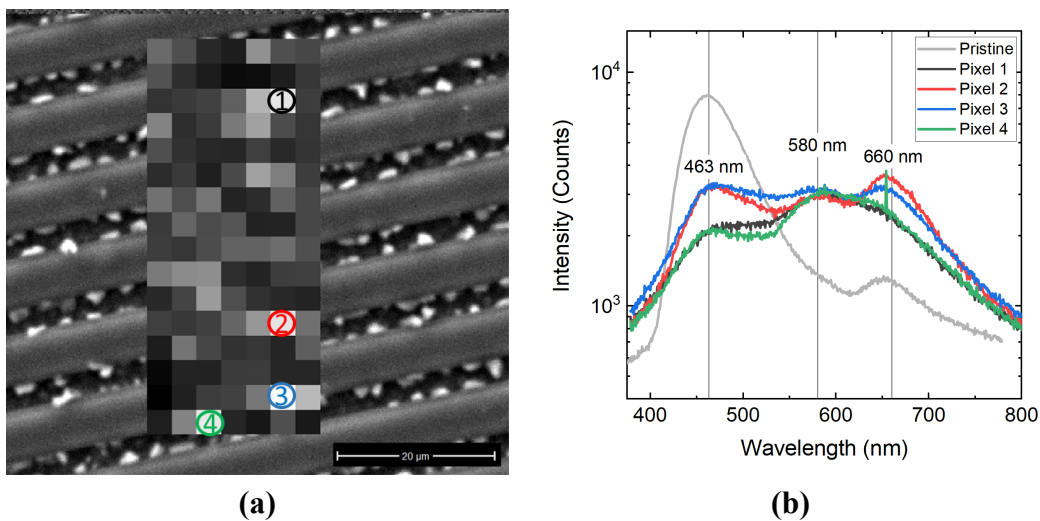


Fig. 3: (a) CL false color map for DUT 1 with pixel sizes of  $3 \times 3 \mu\text{m}^2$ , showing the relative intensity for a 31 nm broad spectral region centered at 575 nm. In (b) the CL spectrum as a function of the wavelength is shown for the four pixels selected in (a) and a pristine reference (in gray).

To highlight the damage induced in DUT 2 by the  $^{131}\text{Xe}^{+35}$  irradiation, the difference between the irradiated and pristine signals has been calculated for each wavelength, considering a pixel size of  $20 \times 20 \mu\text{m}^2$ . Fig. 4 shows the results for Pixels 1 and 3 shown in Fig. 2 (b) (possible ion-tracks) and the pristine reference. Enhanced emission introduced by irradiation is observed between  $\sim 420$  nm and  $\sim 700$  nm, with peaks between  $\sim 455$ - $475$  nm (Pixel 1) and  $\sim 458$ - $480$  nm (Pixel 2). Peaks in this range were previously reported as being characteristics of OVCs ( $\sim 445$ - $480$  nm) and extended defects of different nature (i.e., different types of stacking faults at  $\sim 455$ - $460$  nm and  $\sim 480$  nm [16]). Additional peaks at  $\sim 660$  nm (NBOHCs) and  $\sim 580$  nm (Si-N bonding structures) are visible in the figure inset. Negative values are observed in the near band edge emission of 4H-SiC, which may be indicative of emission quenching by the defects formed by the impinging Xe ions.

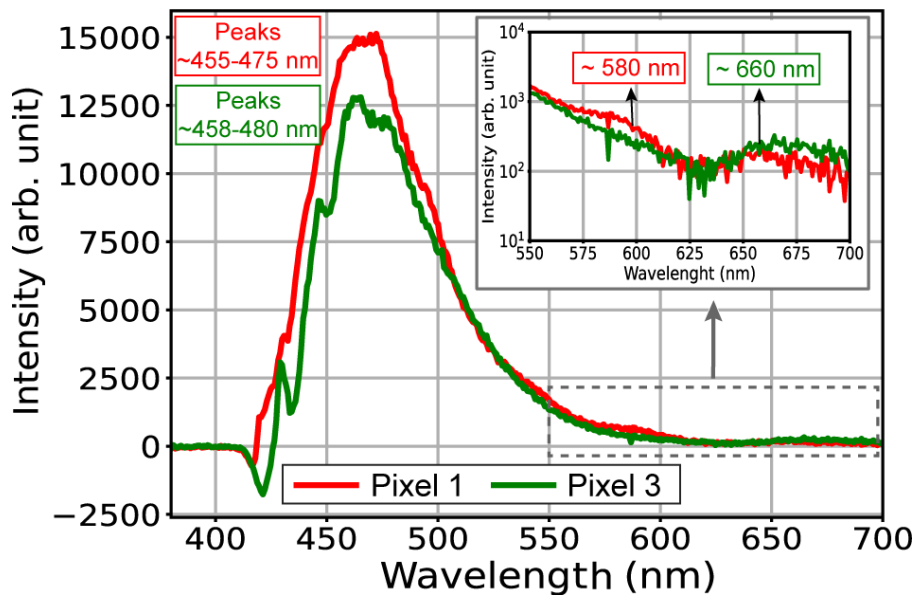


Fig. 4: Difference between the  $^{131}\text{Xe}^{+35}$  irradiated DUT and the pristine signal for Pixel 1-3 as in Fig. 2 (b). The 550-700 nm signal is highlighted in log scale in the figure inset.

## Conclusions

The results show the applicability of CL measurements for investigation of heavy-ion induced damage in SiC power MOSFETs degraded by SELC I and SELC II. Possible ion-tracks have been identified from the analysis of the die surface ( $1 \mu\text{m}$  depth), with larger impact for the device irradiated with  $^{131}\text{Xe}^{+35}$  and degraded with SELC II. Additional features introduced by heavy-ion irradiation were observed for both devices when directly comparing the CL emission with pristine values, such as common luminescence peaks of defect centers localized in thermal-SiO<sub>2</sub>. Higher emission intensity from a defect center causing a peak at  $\sim 580$  nm (possibly related to Si-N) was observed in different regions of the device irradiated with  $^{56}\text{Fe}^{+15}$  and degraded with SELC I. In addition, peaks at the characteristic wavelength of extended defects were identified when subtracting the pristine signal from the signal of the brightest pixels identified as the potential ion tracks for the device degraded with SELC II. Further work is needed to securely identify the defects caused by irradiation, assign the defects to a specific layer within the device stack, and connect them to the degradation seen in the device performance of the DUTs. A stripping away of the oxide layer and cross-section analysis may provide further insights into the defect structures formed in the SiC itself.

---

**References**

- [1] J.-M. Lauenstein, M. C. Casey, R. L. Ladbury, H. S. Kim, A. M. Phan, and A. D. Topper, "Space Radiation Effects on SiC Power Device Reliability," in 2021 IEEE Int. Reliab. Phys. Symp., Mar 2021 (IRPS), pp. 1 – 8.
- [2] D. R. Ball *et al.*, "Ion-induced energy pulse mechanism for single-event burnout in high-voltage SiC power MOSFETs and junction barrier Schottky diodes," IEEE Trans. Nucl. Sci., vol. 67, no. 1, pp. 22-28, Nov. 2019.
- [3] A. F. Witulski *et al.*, "New Insight into Single-Event Radiation Failure Mechanisms in Silicon Carbide Power Schottky Diodes and MOSFETs," Mater. Sci. Forum, vol. 1004, pp. 2019–2030, Jul. 2020.
- [4] C. Martinella *et al.*, "Heavy-ion induced single event effects and latent damages in SiC power MOSFETs," Microelectr. Reliab., vol. 128, 2022.
- [5] A. Javanainen *et al.*, "Heavy ion induced degradation in SiC schottky diodes: bias and energy deposition dependence," IEEE Trans. Nucl. Sci., vol. 64, no. 1, pp. 415-420, Jan. 2017.
- [6] E. Mizuta, S. Kuboyama, H. Abe, Y. Iwata, and T. Tamura, "Investigation of single-event damages on silicon carbide (SiC) power MOSFETs," IEEE Trans. Nucl. Sci., vol. 61, no. 4, pp. 1924–1928, Aug. 2014.
- [7] R. A. Johnson *et al.*, "Analysis of Heavy-Ion-Induced Leakage Current in SiC Power Devices," IEEE Trans. Nucl. Sci., vol. 69, no. 3, pp. 248–253, Mar. 2022.
- [8] C. Martinella *et al.*, "Heavy-ion microbeam studies of Single-Event Leakage Current mechanism in SiC VD-MOSFETs," IEEE Trans Nucl. Sci., vol 66, no. 7, pp. 1381 - 1389, Jun. 2020.
- [9] M. Backman *et al.*, "Molecular dynamics simulations of swift heavy ion induced defect recovery in SiC," Comput. Mater. Sci., vol. 67, pp. 261-265, Feb. 2013.
- [10] A. Javanainen *et al.*, "Molecular dynamics simulations of heavy ion induced defects in SiC schottky diodes," IEEE T Device Mat Re, vol. 18, no. 3, pp 481-483, Sept. 2018.
- [11] P. Chen *et al.*, "Defect Inspection Techniques in SiC," Nanoscale Res. Lett., 17(1), 1–17, Apr. 2021.
- [12] M. Yoshikawa, K. Inoue, H. Seki, Y. Nanen, M. Kato, and T. Kimoto, "Characterization of silicon dioxide films on 4H-SiC (0001) Si, (1-100) M, and (11-20) A faces by cathodoluminescence spectroscopy," Appl. Phys. Lett., 102, 051612, Jan. 2013.
- [13] M. Yoshikawa, *et al.*, "Characterization of silicon dioxide films on 4H-SiC Si (0001) face by cathodoluminescence spectroscopy and x-ray photoelectron spectroscopy," Appl. Phys. Lett., 100(8), 082105, Feb. 2012.
- [14] S. Castelletto, B. C. Johnson, V. Ivády, N. Stavrias, T. Umeda, A. Gali, T. Ohshima, "A silicon carbide room-temperature single-photon source," Nat. Mater., 13:2, 13(2), 151–156, Nov. 2013.
- [15] E. Janzén, A. Gali, P. Carlsson, A. Gällström, B. Magnusson, and N. T. Son, "The silicon vacancy in SiC," Phys. B Condens. Matter, vol. 404, no. 22, pp. 4354–4358, Dec. 2009.
- [16] G. Feng, J. Suda, T. Kimoto, "Triple Shockley type stacking faults in 4H-SiC epilayers," Appl. Phys. Lett., 94, 91910, Mar. 2009.